Electrochemistry Communications 87 (2018) 13–17

Contents lists available at ScienceDirect

Electrochemistry Communications

journal homepage: www.elsevier.com/locate/elecom

Modified Si nanowire/graphite-like carbon nitride core-shell photoanodes for solar water splitting

Minghui Ning[a,c], Zhen Chen[a,c], Lin Li[a,c], Qingguo Meng[b], Zhihong Chen[b,d,*], Yongguang Zhang[d], Mingliang Jin[a,c,d], Zhang Zhang[a,c,d], Mingzhe Yuan[b], Xin Wang[a,c,d,*], Guofu Zhou[a,c,d]

[a] Guangdong Provincial Key Laboratory of Optical Information Materials and Technology & Institute of Electronic Paper Displays, South China Academy of Advanced Optoelectronics, South China Normal University, Guangzhou 510006, PR China
[b] Shenyang Institute of Automation, Chinese Academy of Sciences, Guangzhou, 511458, PR China
[c] National Center for International Research on Green Optoelectronics, South China Normal University, Guangzhou 510006, PR China
[d] International Academy of Optoelectronics at Zhaoqing, South China Normal University, Guangdong Province, PR China

ARTICLE INFO

Keywords:
Water splitting
Si nanowires
Graphite-like carbon nitride
Core/shell nanostructure
Copolymerization modification

ABSTRACT

Si nanowires (SiNWs) and graphite-like carbon nitride (g-C_3N_4) are highly promising materials for solar water splitting. In this work, n-type SiNWs (n-SiNWs) are obtained via metal-catalyzed electroless etching. To improve the photoelectrochemical performance of the n-SiNWs, g-C_3N_4 is deposited on their surface as a coating layer (n-SiNW/g-C_3N_4). Furthermore, to increase the density of active sites in g-C_3N_4, barbituric acid (BA) is introduced into precursors before the layer deposition. The n-SiNW/g-C_3N_4 photoanode shows a negative shift of the onset potential as compared to the bare n-SiNWs. Moreover, a 50% enhancement in the photocurrent density at 1.6 V vs. RHE is achieved on the BA-modified n-SiNW/g-C_3N_4 as compared to the pristine n-SiNW/g-C_3N_4.

1. Introduction

Solar water splitting is a promising method for solar energy utilization because it allows for the direct conversion of solar energy into chemical energy that is stored within oxygen and hydrogen [1–6]. Silicon is a small-band gap semiconductor that is capable of absorbing most of the sunlight in the visible range, but it generates insufficient photovoltage for water splitting [7–13]. Because of its unique properties, graphite-like carbon nitride (g-C_3N_4) was considered an ideal candidate for solar-driven water splitting [14–16]. However, due to its relatively large band gap (2.7 eV), g-C_3N_4 does not absorb most of the visible light, which includes a large portion of the solar energy [17,18].

A possible solution to address the aforementioned shortcomings of these two materials is to combine them and design a rational solar water splitting device based on the synergistic effect between Si and g-C_3N_4. Specifically, Si nanowires (SiNWs) has a high specific surface area and strong light trapping ability [19–23]. In recent years, numerous reports on the use of SiNWs in solar water splitting have been published. Cai et al. fabricated $Fe_xNi_{1-x}O/Bi_2MoO_6$/SiNWs via a facile and novel process, and these NWs exhibited an STH up to 0.27% [24]. Moreover, the metal-free SiNW photoelectrodes reported by Halima et al. achieved a photovoltage of 250 mV under illumination [11]. In this work, g-C_3N_4 was deposited on the top of n-SiNWs form a core-shell heterojunction. This core-shell heterostructure enabled the photoelectrochemical (PEC) photoanode to absorb most of the sunlight, so that H_2O could be decomposed at a low bias.

The PEC performance of pristine g-C_3N_4 is strongly limited by the sluggish carrier kinetics resulting from the insufficient surface active sites [18,25]. Hence, we applied barbituric acid (BA) to modify the properties of g-C_3N_4 through copolymerization [26]. The g-C_3N_4 modified by BA is denoted as CNB_x, and the modified electrode is denoted n-SiNW/CNB_x.

2. Experimental

2.1. Fabrication of n-SiNW/g-C_3N_4 core-shell structure

The n-SiNW arrays were synthesized via MCEE, which was developed by Peng et al. [27]. Si pieces (2 × 2 cm^2) were ultrasonically cleaned with acetone and ethanol, boiled in H_2SO_4:H_2O_2 (3:1) solution for 30 min, and then rinsed with DI water several times to remove the residues. To obtain SiNW arrays, the cleaned wafers were sealed in an autoclave that contained 5 M HF and 0.02 M $AgNO_3$ solution. The SiNW arrays were immersed in nitric acid for 30 min to remove Ag. After removal of the oxide layers with 4% HF and subsequent drying in air, different amounts of the precursor (50, 90, 180 and 300 μL

* Corresponding authors at: National Center for International Research on Green Optoelectronics, Shenyang Institute of Automation, Guangzhou.
E-mail addresses: chenzhihong1227@sina.com (Z. Chen), wangxin@scnu.edu.cn (X. Wang).

https://doi.org/10.1016/j.elecom.2017.12.010
Received 24 November 2017; Accepted 9 December 2017
Available online 11 December 2017

dicyandiamide) were dipped on the surface of the SiNW arrays, which were left to dry at room temperature under dark and ventilated conditions. Then, the arrays were placed in a vacuum tube furnace, and the temperature was increased from 20 °C to 550 °C at the rate of 3 °C/min. The temperature was maintained at 550 °C for 4 h for the fabrication of the n-SiNW/g-C_3N_4 core-shell structure. The n-SiNW array with 90 μL of the precursor exhibited the most promising PEC performance.

2.2. Fabrication of n-SiNW/CNB_x core-shell structure

n-SiNW/CNB_x photoanodes were fabricated using the same method as that for the n-SiNW/g-C_3N_4 photoanodes, but the precursors were changed to BA and dicyandiamide solutions. Different amounts of BA and 2 g of dicyandiamide were simultaneously added to 30 mL of deionized water to obtain the new precursors. The concentrations of BA were set as 1.3, 2.6, 5.2, 10.4, 26.0, 52.0 and 520 mM, corresponding to $CNB_{0.0025}$, $CNB_{0.005}$, $CNB_{0.01}$, $CNB_{0.02}$, $CNB_{0.05}$ and CNB_1 respectively.

3. Results and discussion

3.1. Structural characterization and composition analysis

The photoanodes prepared by loading 90 μL of the precursor were considered, unless specified otherwise. Scanning electron microscopy (SEM) and transmission electron microscopy (TEM) images of the n-SiNW/$CNB_{0.02}$ photoanode are shown in Fig. 1. From Fig. 1a, b, and d, the length and diameter of the nanowires in n-SiNW/$CNB_{0.02}$ are found to be approximately 4 μm and 120 nm. The TEM images in Fig. 1c and d indicate that the thickness of the $CNB_{0.02}$ is about 20 nm. X-ray photoelectron spectroscopy (XPS) measurements are shown in Fig. 2 to illustrate the chemical composition and chemical states of the samples. Fig. 2a shows the survey XPS spectra of n-SiNW/$CNB_{0.02}$. The relatively low peak intensities of C 1 s and N 1 s can be ascribed to the low loading amount and the well-dispersed $CNB_{0.02}$. Fig. 2a suggests the coexistence of n-SiNW and $CNB_{0.02}$ in n-SiNW/$CNB_{0.02}$. Fig. 2b displays high-resolution Si 2p spectrum of n-SiNW/$CNB_{0.02}$, revealing the presence of two peaks at 98.9 and 103.0 eV, which is attributable to Si and its oxide species. N-SiNW/CNB_1 was fabricated to more distinctly analyze the difference between n-SiNW/g-C_3N_4 and n-SiNW/CNB_x. In Fig. 2c, the peak located at 284.9 eV corresponds to the C—C bond for n-SiNW/g-C_3N_4 and n-SiNW/CNB_1. The peak at 287.5 eV of n-SiNW/g-C_3N_4 can be associated with the C—N bond [28]. The corresponding peak of n-SiNW/CNB_1 shifted to 287.0 eV, indicating the chemical change of CNB_1. Three distinct peaks can be observed from Fig. 3c; the peaks located at 397.9 eV, 398.7 eV, and 400.1 eV correspond to the C—N═C, N—$(C)_3$, and C—N—H bond, respectively [29,30]. The slightly peak shifts of N 1 s compared to other reported literatures can be ascribed to the ultra-thin shell structure and the interaction with SiNW. With the introduction of BA, CNB_1 exhibits higher peak intensity at 397.9 eV and 398.7 eV, indicating the C/N ratio of n-SiNW/CNB_1 is larger than the n-SiNW/g-C_3N_4. These results strongly confirm that certain N atoms in g-C_3N_4 are replaced by the C atoms in CNB_1, i.e. N-defects [29–31].

3.2. Analysis of photoelectrochemical performance

As shown by the LSV measurements in Fig. 3a, the photoanode fabricated with 90 μL of the precursor delivered the most promising PEC performance. It could be attributed to CNB_x with N-defects which exhibited enhanced charge collection and electron-hole separation abilities compared with g-C_3N_4 [26,30]. Therefore, the N-defects could act as active OER sites in CNB_x. However, it is also reported excessive BA doping would hinder photocatalytic performance of CNB_x [26,30]; hence, the amount of BA was studied in this work. From Fig. 3b, the optimal amount of BA corresponds to $CNB_{0.02}$. The photovoltages of the bare n-SiNWs, n-SiNW/g-C_3N_4 and n-SiNW/$CNB_{0.02}$ were 200 mV, 270 mV, and 310 mV respectively. Fig. 3c illustrates the LSV results for the bare n-SiNWs, n-SiNW/g-C_3N_4, and n-SiNW/$CNB_{0.02}$ photoanodes. The addition of g-C_3N_4 induced a negative shift of the onset potential of the n-SiNW/g-C_3N_4 photoanode as compared to that for the bare n-SiNWs, because of the promoted photovoltage. The n-SiNW/$CNB_{0.02}$ photoanode showed 50% enhancement in the photocurrent density at 1.61 V vs. RHE, over that of the n-SiNW/g-C_3N_4 photoanode. The high photocurrent could be ascribed to the N-defects that further promoted charge separation and increased the active OER sites on the surface of $CNB_{0.02}$. To reveal the contribution of photocurrent from different materials, an additional 420 nm cutoff filter was used to remove any light below 420 nm; the LSV data of the samples are showed in Fig. 3c. With the 420 nm cutoff filter introduced, the n-SiNW/g-C_3N_4 shows a similar photocurrent with n-SiNW, suggesting that the photocurrents of n-SiNW of n-SiNW/g-C_3N_4 mainly originated from SiNW when the

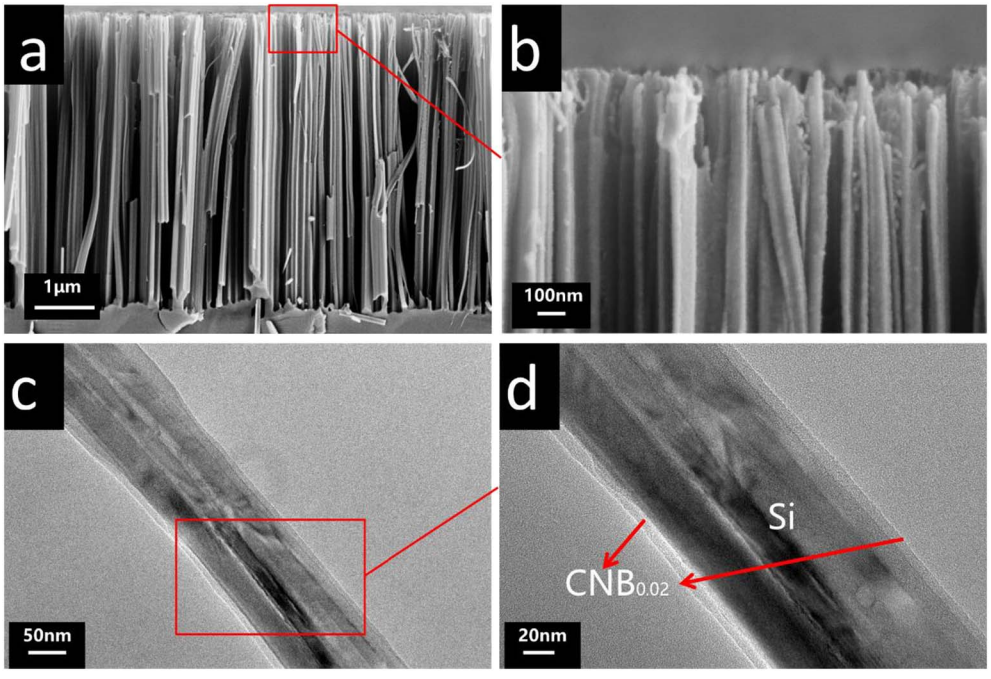

Fig. 1. Structural characterization of n-SiNW/$CNB_{0.02}$ photoanode. (a)(b) SEM cross-sectional image of n-SiNW/$CNB_{0.02}$ photoanode under different resolutions. (c)(d) TEM image of n-SiNW/$CNB_{0.02}$ nanowire under different resolutions.

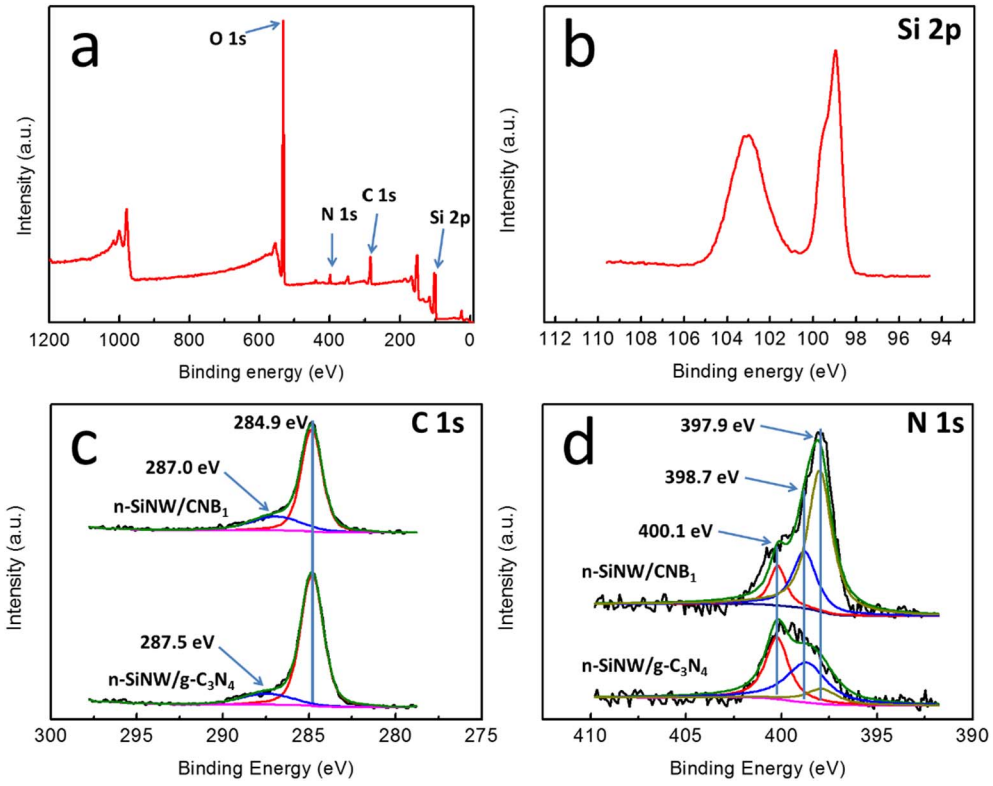

Fig. 2. (a) XPS survey spectrum of n-SiNW/$CNB_{0.02}$, (b) Si 2p XPS spectra of n-SiNW/$CNB_{0.02}$, (c) C 1s XPS spectra of n-SiNW/g-C_3N_4 and n-SiNW/CNB_1, (d) N 1s XPS spectra of n-SiNW/g-C_3N_4 and n-SiNW/CNB_1.

irradiated light wavelength is larger than 420 nm. Under AM 1.5 light irradiation, the n-SiNW/g-C_3N_4 and n-SiNW/$CNB_{0.02}$ showed much higher enhancement photocurrents than that of n-SiNW, which indicate that the photocurrents of n-SiNW/g-C_3N_4 were mainly originated from Si/g-C_3N_4 and Si/$CNB_{0.02}$. Interestingly, with or without 420 nm cutoff filter introduction, n-SiNW/$CNB_{0.02}$ exhibited enhanced photocurrent with compare of n-SiNW/g-C_3N_4, which might be contributed by the enhanced light absorbance and promoted charge separation caused by the introduction of N-defects. To further prove the function of N-defects, we also tested the minor carrier life time of n-SiNW/$CNB_{0.02}$ and n-SiNW/g-C_3N_4. The n-SiNW/$CNB_{0.02}$ (24.54 μs) shows a slightly longer minor carrier life time than and n-SiNW/g-C_3N_4 (24.13 μs), implying that the introduction of N-defects could indeed improve charge separation efficiency and thus enhance the carrier life time of n-SiNW/$CNB_{0.02}$. G-C_3N_4 and $CNB_{0.02}$ were deposited on FTO, and LSV data were obtained under chopped light to clarify the relationship between the N-defects and active OER sites. The data are shown in Fig. 3d. $CNB_{0.02}$/FTO exhibited better PEC performance than g-C_3N_4/FTO, which strongly indicated that the introduced N-defects could act as active OER sites.

The applied bias photon-to-current efficiency of n-SiNW/$CNB_{0.02}$ was measured and reached the highest value of 0.278% with bias of 0.52 V. Compared with other excellent Si-based photoelectrodes such as a-Si:H/a-Si:H/mc-Si:H, whose efficiency is close to 10% [32], the n-SiNW/$CNB_{0.02}$ shows a lower efficiency. Nonetheless, the synthesis of n-SiNW/$CNB_{0.02}$ is more facile and cost-effective. Besides, the PEC performance of n-SiNW/$CNB_{0.02}$ can be further improved, which will be analyzed in a future study.

Fig. 3d shows the LSV curves under illumination with chopped light, where quick photocurrent response is observed. Fig. 3e shows the J-t curves (300 s, under a bias of 1.11 V vs. RHE) obtained under chopped light. The photostability of the as-prepared photoanodes was studied in Fig. 3e. The photoanodes showed about 80% decayed photocurrents as compared with pristine photocurrents (Fig. 3e). The slight decay in the photocurrent of the J-t curves was mainly due to the mild photocorrosion during illumination. Our n-SiNW/g-C_3N_4 core/shell structure offers similar results as those observed in the photoelectrochemical water splitting using the C_3N_4-based core/shell structure reported by Li et al. In that study, TiO_2 and WO_3 were applied as the core materials, which led to remarkable performance [33,34]. Because of the unique advantages of SiNWs, such as better charge transfer ability on account of the direct inheriting from the bulk substrate and the strong light trapping ability due to its rough surface, solar-driven water splitting can be achieved under lower bias voltage which could be consider as a great advance for this structure.

3.3. Electrochemical analyses

Electrochemical analyses were conducted by EIS measurements to investigate the electrical properties and charge transfer process of the photoanodes. As seen in Fig. 3f, the EIS Nyquist curve of the bare n-SiNWs shows a larger arc with respect to n-SiNW/g-C_3N_4, indicating enhanced charge transfer ability in the latter because of the strong charge separation at the g-C_3N_4/Si interface. Meanwhile, the Nyquist curve of n-SiNW/$CNB_{0.02}$ also exhibits a smaller arc than that for n-SiNW/g-C_3N_4, suggesting that the resistance of the former is reduced after modification with BA, probably because of the introduction of N-defects. The electrochemical data well agree with the PEC performance, further confirming our previous conclusions.

4. Conclusion

We successfully coated the surface of n-SiNWs with g-C_3N_4 by LALD. N-SiNW/g-C_3N_4 exhibited a cathodic shift of the onset potential and larger photocurrent as compared to the bare n-SiNWs. Subsequently, BA was applied to modify the g-C_3N_4 properties through copolymerization; therefore, the PEC performance was further enhanced for the n-SiNW/$CNB_{0.02}$ photoanode. Further research was carried out to evaluate the electrical properties and charge transfer ability of the photoanodes, and the results were consistent with those of the PEC results. This work confirms the highly promising potential of the core/shell nanoheterostructure for enhancing the photovoltage and modifying surface states

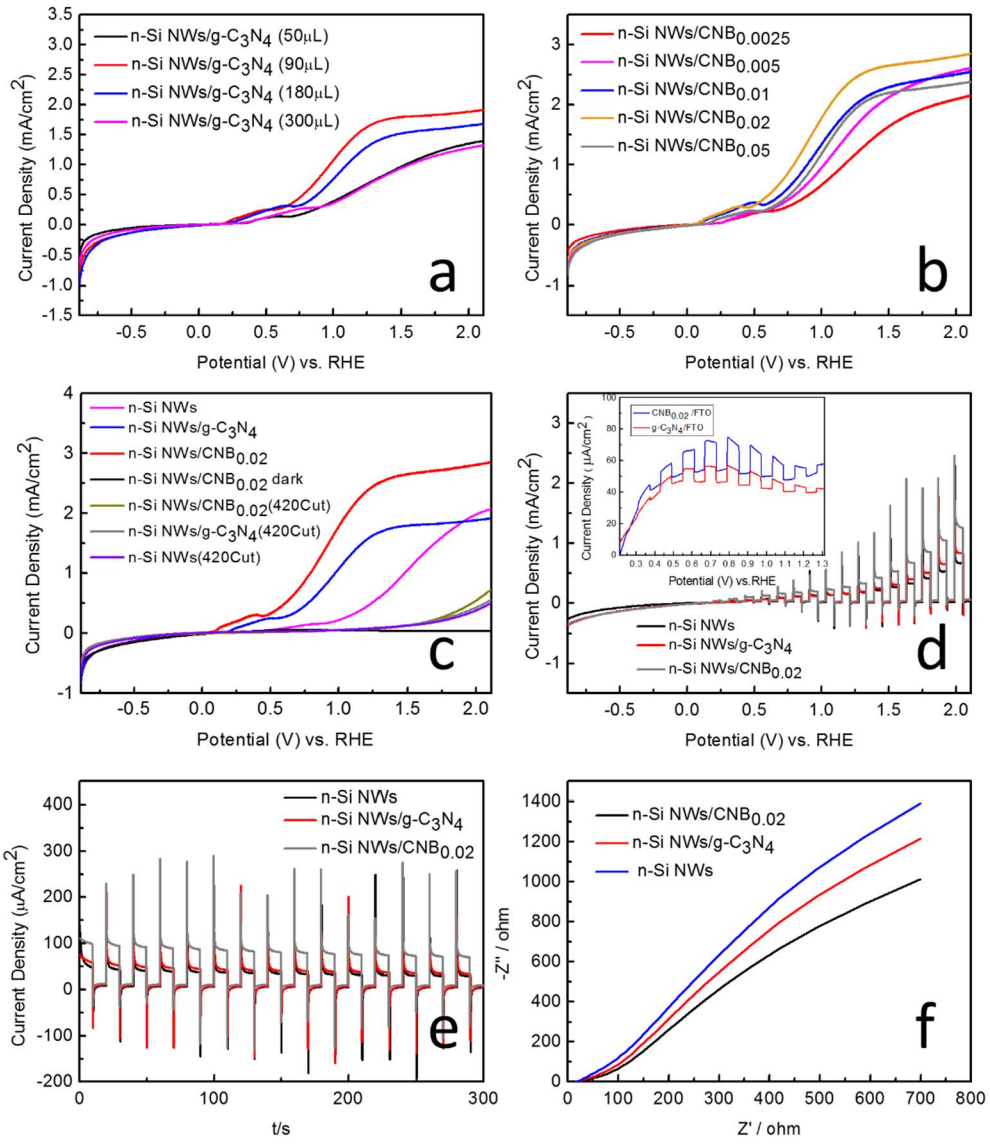

Fig. 3. (a) LSV curves of n-SiNW/g-C_3N_4 with different precursors, (b) LSV curves of n-SiNW/CNB_x, (c) LSV curves of different photoanodes, (d) LSV curves of transient response, (e) J-t curves of transient response, (f) EIS Nyquist plots.

through the incorporation of active sites, so that superior efficiency could be achieved in PEC water-splitting applications.

Acknowledgements

The authors acknowledge the financial support from the NSFC (Grant No. 51602111, 51561135014, U1501244), Xijiang R&D team (X Wang), National Key R&D Program of China (2016YFB0401502), Guangdong Provincial Grant (2015A030310196, 2014B090915005, 2015B090913004), the Pearl River S&T Nova Program of Guangzhou (201506040045), CAS Hundred Talent Program, Nansha International S&T Cooperation Program (2016GJ005), Guangdong Provincial Science and Technology Project (2017A050506009), LOIT (Grant No. 2017B030301007), MOE International Laboratory for Optical Information Technologies and 111 Project.

References

[1] M.G. Walter, E.L. Warren, J.R. McKone, S.W. Boettcher, Q. Mi, E.A. Santori, N.S. Lewis, Solar water splitting cells, Chem. Rev. 110 (2010) 6446–6473.
[2] X. Chen, S. Shen, L. Guo, S.S. Mao, Semiconductor-based photocatalytic hydrogen generation, Chem. Rev. 110 (2010) 6503–6570.
[3] S. Kment, F. Riboni, S. Pausova, L. Wang, L. Wang, H. Han, Z. Hubicka, J. Krysa, P. Schmuki, R. Zboril, Photoanodes based on TiO_2 and α-Fe_2O_3 for solar water splitting-superior role of 1D nanoarchitectures and of combined heterostructures, Chem. Soc. Rev. 46 (2017) 3716–3769.
[4] J. Luo, L. Steier, M.K. Son, M. Schreier, M.T. Mayer, M. Grätzel, Cu_2O nanowire photocathodes for efficient and durable solar water splitting, Nano Lett. 16 (2016) 1848–1857.
[5] Y.Y. Zhang, Y.X. Tang, X.F. Liu, Z.L. Dong, H.H. Hng, Z. Chen, T.C. Sum, X.D. Chen, Three-dimensional CdS–Titanate composite nanomaterials for enhanced visible-light-driven hydrogen evolution, Small 9 (2013) 996–1002.
[6] X.T. Wang, C. Liow, A. Bisht, X.F. Liu, T.C. Sum, X.D. Chen, S.Z. Li, Engineering interfacial photo-induced charge transfer based on nanobamboo array architecture for efficient solar-to-chemical energy conversion, Adv. Mater. 27 (2015) 2207–2214.
[7] K.Q. Peng, X. Wang, S.T. Lee, Silicon nanowire array photoelectrochemical solar cells, Appl. Phys. Lett. 92 (2008) 163103.
[8] I. Oh, J. Kye, S. Hwang, Enhanced photoelectrochemical hydrogen production from silicon nanowire array photocathode, Nano Lett. 12 (2012) 298–302.
[9] H. Zhang, Q. Ding, D. He, H. Liu, W. Liu, Z. Li, B. Yang, X. Zhang, L. Lei, S. Jin, A p-Si/$NiCoSe_x$ core/shell nanopillar array photocathode for enhanced photoelectrochemical hydrogen production, Energy Environ. Sci. 9 (2016) 3113–3119.
[10] X. Wang, K.Q. Peng, X. Wu, S.T. Lee, Single crystalline ordered silicon wire/Pt nanoparticle hybrids for solar energy harvesting, Electrochem. Commun. 12 (2010) 509–512.
[11] A.F. Halima, X. Zhang, D.R. MacFarlane, Metal-free black silicon for solar-powered hydrogen generation, Electrochim. Acta 235 (2017) 453–462.
[12] F. Chen, Q. Zhu, Y. Wang, W. Cui, X. Su, Y. Li, Efficient photoelectrochemical hydrogen evolution on silicon photocathodes interfaced with nanostructured NiP_2 cocatalyst films, ACS Appl. Mater. Interfaces 8 (2016) 31025–31031.
[13] M.V. Sheridan, D.J. Hill, B.D. Sherman, D. Wang, S.L. Marquard, K.R. Wee, J.F. Cahoon, T.J. Meyer, All-in-one derivatized tandem p + n-Silicon − SnO_2/TiO_2

water splitting photoelectrochemical cell, Nano Lett. 17 (2017) 2440–2446.
[14] X.C. Wang, K. Meada, A. Thomas, K. Takanabe, G. Xin, J.M. Carlsson, K. Domen, M. Antonietti, A metal-free polymeric photocatalyst for hydrogen production from water under visible light, Nat. Mater. 8 (2009) 76–80.
[15] G.G. Zhang, Z.A. Lan, L.H. Lin, S. Lin, X.C. Wang, Overall water splitting by Pt/g-C_3N_4 photocatalysts without using sacrificial agents, Chem. Sci. 7 (2016) 3062–3066.
[16] Z. Chen, G. Ma, Z.H. Chen, Y.G. Zhang, Z. Zhang, J.W. Gao, Q.G. Meng, M.Z. Yuan, X. Wang, J.M. Liu, G.F. Zhou, Fabrication and photoelectrochemical properties of silicon nanowires/g-C_3N_4 core/shell arrays, Appl. Surf. Sci. 396 (2017) 609–615.
[17] H.M. Wang, X.X. Li, J.L. Yang, The g-C_3N_4/C_2N nanocomposite: a g-C_3N_4-based water-splitting photocatalyst with enhanced energy efficiency, ChemPhysChem 17 (2016) 2100–2104.
[18] R.Q. Ye, H.B. Fang, Y.Z. Zheng, N. Li, Y. Wang, X. Tao, Fabrication of $CoTiO_3$/g-C_3N_4 hybrid photocatalysts with enhanced H_2 evolution: z-scheme photocatalytic mechanism insight, ACS Appl. Mater. Interfaces 8 (2016) 13879–13889.
[19] D. Liu, L.L. Li, Y. Gao, C.M. Wang, J. Jiang, Y.J. Xiong, The nature of photocatalytic "water splitting" on Silicon nanowires, Angew. Chem. Int. Ed. 54 (2015) 2980–2985.
[20] D.H. Lee, S.P.R. Kobaku, Y.R. Hong, J.Y. Kwon, An efficient photoelectrochemical hydrogen evolution system using Silicon nanomaterials with ultra-high aspect ratios, Energy Technol. 2 (2014) 889–896.
[21] X. Wang, K.Q. Peng, Y. Hu, F.Q. Zhang, B. Hu, L. Li, M. Wang, X.M. Meng, S.T. Lee, Silicon/hematite core/shell nanowire array decorated with gold nanoparticles for unbiased solar water oxidation, Nano Lett. 14 (2014) 18–23.
[22] Z. Chen, M.H. Ning, G. Ma, Q. Meng, Y. Zhang, J. Gao, M. Jin, Z. Chen, M. Yuan, X. Wang, J.M. Liu, G.H. Zhou, Effective silicon nanowire arrays/WO_3 core/shell photoelectrode for neutral pH water splitting, Nanotechnology 28 (2017) 275401.
[23] X. Wang, K.Q. Peng, X.J. Pan, X. Chen, Y. Yang, L. Li, X.M. Meng, W.J. Zhang, S.T. Lee, High-performance silicon nanowire array photoelectrochemical solar cells through surface passivation and modification, Angew. Chem. Int. Ed. 50 (2011) 9861–9865.
[24] Z.X. Cai, F.M. Li, W. Xua, Y.Q. Jiang, F. Luo, Y.R. Wang, X. Chen, Enhanced performance of photoelectrochemical water oxidation using three-dimensional interconnected nanostructural photoanode via simultaneously harnessing charge transfer and coating with an oxygen evolution catalyst, Nano Energy 26 (2016) 257–266.
[25] Y. Zheng, L.H. Lin, B. Wang, X.C. Wang, Graphitic carbon nitride polymers toward sustainable photoredox catalysis, Angew. Chem. Int. Ed. 54 (2015) 12868–12884.
[26] J. Zhang, X. Chen, K. Takanabe, K. Maeda, K. Domen, J.D. Epping, X. Fu, M. Antonietti, X. Wang, Synthesis of a carbon nitride structure for visible-light catalysis by copolymerization, Angew. Chem. Int. Ed. 49 (2010) 441–444.
[27] K.Q. Peng, Y.J. Yan, S.P. Gao, J. Zhu, Synthesis of large-area Silicon nanowire arrays via self-assembling nanoelectrochemistry, Adv. Mater. 14 (2002) 1164.
[28] Q. Liu, T.X. Chen, Y.R. Guo, Z.G. Zhang, X.M. Fang, Ultrathin g-C_3N_4 nanosheets coupled with carbon nanodots as 2D/0D composites for efficient photocatalytic H2 evolution, Appl. Catal. B Environ. 193 (2016) 248–258.
[29] E. Vorobyeva, Z. Chen, S. Mitchell, R.K. Leary, P. Midgley, J.M. Thomas, R. Hauert, E. Fako, N. Lopez, J. Perez-Ramirez, Tailoring the framework composition of carbon nitride to improve the catalytic efficiency of the stabilised palladium atoms, J. Mater. Chem. A 5 (2017) 16393–16403.
[30] J.N. Qin, S.B. Wang, H. Ren, Y.D. Hou, X.C. Wang, Photocatalytic reduction of CO_2 by graphitic carbon nitride polymers derived from urea and barbituric acid, Appl. Catal. B Environ. 179 (2015) 1–8.
[31] H.J. Yu, R. Shi, Y.X. Zhao, T. Bian, Y.F. Zhao, C. Zhou, G.I.N. Waterhouse, L.-Z. Wu, C.-H. Tung, T.R. Zhang, Alkali-assisted synthesis of nitrogen deficient graphitic carbon nitride with tunable band structures for efficient visible-light-driven hydrogen evolution, Adv. Mater. 29 (2017) 1605148.
[32] F. Urbain, V. Smirnov, J.P. Becker, A. Lambertz, F. Yang, J. Ziegler, B. Kaiser, W. Jaegermann, U. Rau, F. Finger, Multijunction Si photocathodes with tunable photovoltages from 2.0 V to 2.8 V for light induced water splitting, Energy Environ. Sci. 9 (2016) 145–154.
[33] Y.G. Li, R.R. Wang, H.J. Li, X.L. Wei, J. Feng, K.Q. Liu, Y.Q. Dang, A.N. Zhou, Efficient and stable photoelectrochemical seawater splitting with TiO_2@g-C_3N_4 nanorod arrays decorated by Co-Pi, J. Phys. Chem. C 119 (2015) 20283–20292.
[34] Y.G. Li, X.L. Wei, X.Y. Yan, J.T. Cai, A.N. Zhou, M.R. Yang, K.Q. Liu, Construction of inorganic–organic 2D/2D WO_3/g-C_3N_4 nanosheet arrays toward efficient photoelectrochemical splitting of natural seawater, Phys. Chem. Chem. Phys. 18 (2016) 10255–10261.